REFERENCES

[1] Y.-J Hwang, C.-H. Lien, H. Wang, and M. W. Sinclair, “A 78–114 GHz Monolithic Subharmonically Pumped GaAs-Based HEMT Diode Mixer,” *IEEE Microwave and Wireless Components Lett.*, vol. 12, pp. 209-211, Jun. 2002.

[2] K. C. Gupta, R. Garg, I. Bahl, and P. Bhartia, *Microstrip Lines and Slotlines*. Norwood, MA: Artech House, 1996.

[3] K. Nishikawa, S. Sugitani, K. Inoue, T. Ishii, K. Kamogawa, B. Piernas and K. Araki, "Low- loss passive components on BCB- based 3D MMIC technology." *IEEE MTT- S Int. Microwave Symp. Dig.*, 2001, pp. 1881-1884.

[4] G. L. Matthaei, S. M. Rohlfing, R. J. Forse,” Design of HTS, lumped-element, manifold-type microwave multiplexers”, *IEEE Trans. Microwave Theory Tech.* vol. 44, pp.1313-1321, July 1997.

[5] T. Nakatsuka, J. Itoh, S. Yamamoto, T. Yoshida, M. Nishitsuji, T. Uda, K. Nishii, and O. Ishikawa, “ A highly miniaturized receiver front-end hybrid IC using on-chip high-dielectric constant capacitors for mobile communication equipment,” in *IEEE Microwave and Millimeter-Wave Monolithic Circuits Symp.*, 1995, pp. 85-88.

[6] H. Matsumoto, H. Ogura, and T. Nishikawa, “A miniaturized dielectric monoblock band-pass Filter for 800 MHz band cordless telephone system,” in *IEEE MTT-S Int. Microwave Symp. Dig.*, 1994, pp. 249-252.

[7] H. Matsumoto, T. Tsujiguchi, and T. Nishikawa, “A miniaturized dielectric monoblock duplexer matched by the buried impedance transforming Circuit,” in *IEEE MTT-S Int. Microwave Symp. Dig.*, 1995, pp. 1539-1542.

[8] R. K. Hoffmann, *Handbook of Microwave Integrated Circuits*, Norwood, MA: Artech House, 1987.

[9] Y. Ishikawa, T. Okada, S. Shinmura, F. Kanaya, K. Wakino, and T. Nishikawa, “A miniaturized low-spurious 1.9 GHz MSW band-pass filter using YIG resonators with multi metal rings,” in *IEEE MTT-S Int. Microwave Symp. Dig.*, 1992, pp. 1403-1406.

[10] H. Ogawa and T. Itoh, “Slow-wave characteristics of ferromagnetic semiconductor microstrip line,” *IEEE Trans. Microwave Theory Tech.*, vol. MTT-34, pp. 1478-1482, Dec. 1986.

[11] D. Jäger, “Slow-wave propagation along variable Schottky-contact microstrip line,” *IEEE Trans. Microwave Theory Tech.*, vol. MTT-24, pp. 566-573, Sep. 1976.

[12] H. Ogawa and T. Itoh, “Slow-wave characteristics of ferromagnetic semiconductor microstrip line,” *IEEE Trans. Microwave Theory Tech.*, vol. MTT-34, pp. 1478-1482, Dec. 1986.

[13] F.–R. Yang, K.–P. Ma, Y. Qian, and T. Itoh, “A uniplanar compact photonic-bandgap (UC-PBG) structure and its applications for microwave circuits,” *IEEE Trans. Microwave Theory Tech.*, vol. 47, pp. 1509-1514, Aug. 1999.

[14] C.-K. Wu, H.-S. Wu, and C.-K. C. Tzuang, “Electric-magnetic-electric slow-wave microstrip line and bandpass filter of compressed size,” *IEEE Trans. Microwave Theory Tech.*, vol. 50, pp. 1996-2004, Aug. 2002.

[15] T. Tokumitsu, T. Hiraoka, H. Nakamoto, and T. Takenaka, “Multilayer MMIC using a 3 μm × 3-layer dielectric film structure,” in *IEEE MTT-S Int. Microwave Symp. Dig.*, 1990, pp. 831-834.

[16] T. Hiraoka, T. Tokumitsu, and M. Aikawa, “Very small wide-band MMIC

magic T's using microstrip lines on a thin dielectric film," *IEEE Trans. Microwave Theory Tech.*, vol. 37, pp. 1569-1575, Oct. 1989.

[17] T. Tokumitsu, M. Hirano, K. Yamasaki, C. Yamaguchi, K. Nishikawa, and M. Aikawa, "Highly integrated three-dimensional MMIC technology applied to novel masterslice GaAs- and Si-MMIC's," *IEEE J. Solid-State Circuits*, vol. 32, pp. 1334–1341, Sept. 1997.

[18] K. Nishikawa, K. Kamogawa, K. Inoue, K. Onodera, T. Tokumitsu, M. Tanaka, I. Toyoda, and M. Hirano, "Miniaturized millimeter-wave masterslice 3-D MMIC amplifier and mixer," *IEEE Trans. Microwave Theory Tech.*, vol. 47, pp. 1856–1862, Sept. 1999.

[19] C. Warns, W. Menzel, and H. Schumacher, "Transmission lines and passive elements for multilayer coplanar circuits on silicon," *IEEE Trans. Microwave Theory Tech.*, vol. 46, pp. 616-622, May 1998.

[20] K. Wu, R. Vahldieck, J. L. Fikart, and H. Minkus, "The influence of finite conductor thickness and conductivity on fundamental and higher-order modes in miniature hybrid MIC's (MHMIC's) and MMIC's," *IEEE Trans. Microwave Theory Tech.*, vol.41, pp. 421-430, Mar. 1993.

[21] S. Banba and H. Ogawa, "Small-sized MMIC amplifiers using Thin dielectric layers," *IEEE Trans. Microwave Theory Tech.*, vol. 43, pp. 485-492, Mar. 1995.

[22] T. Imaoka, S. Banba, A. Minakawa, and N. Imai, "Millimeter-wave wide-band amplifiers using multilayer MMIC technology," *IEEE Trans. Microwave Theory Tech.*, vol. 45, pp. 95-101, Jan. 1997.

[23] W. P. Harokopus, Jr., and L. P. B. Katehi, "Electromagnetic coupling and radiation loss considerations in microstrip (M)MIC design," *IEEE Trans. Microwave Theory Tech.*, vol. 39, pp. 413-421, Mar. 1991.

[24] N. Jain and P. Onno, " Methods of using commercial electromagnetic

simulators for microwave and millimeter-wave circuit design and optimization," *IEEE Trans. Microwave Theory Tech.*, vol. 45, pp. 724-746, May 1997.

[25] A. K. Agrawal and G. F. Mikucki, "A printed circuit hybrid-ring directional coupler for arbitrary power divisions," in *IEEE MTT-S Int. Microwave Symp. Dig.*, 1986, pp. 139-142.

[26] R. Levy and L. F. Lind, "Synthesis of symmetrical branch-guide directional couplers," *IEEE Trans. Microwave Theory Tech.*, vol. MTT-16, pp. 80-89, Feb. 1968.

[27] C. Quendo, E. Rius, C. Person, and M. Ney, "Integration of optimized low-pass filters in a bandpass filter for out-of-band improvement," *IEEE Trans. Microwave Theory Tech.*, vol. 49, pp. 2376-2383, Dec. 2001.

[28] Y. Yamada, Y. Ebine and K. Tsunekawa, " Base and mobile station antennas for land mobile radio system," *IEICE Trans. Japan*, vol. E74, no. 6, pp. 1547- 1555, 1991.

[29] K. Ogawa and T. Uwano," A variable tilted fan beam antenna for indoor base stations," *IEEE Intl. Antennas Propag. Symp. Dig.*, 1994, vol. 1, pp. 332-335.

[30] R. A. York and T. Itoh," Injection- and phase-locking techniques for beam control," *IEEE Trans. Microwave Theory and Tech.*, MTT-46, pp. 1920-1929, Nov. 1998.

[31] Y. Qian, B. C. C. Chang, M. F. Chang and T. Itoh," Reconfigurable leaky-mode / multifunction patch antenna structure," *Electron. Lett.*, vol. 35, no. 2, pp. 104-105, Jan. 1999.

[32] A. Henderson, J. R. James, A. Frag and G. D. Evans," New ideas for beam scanning using magnetized ferrite," *Electronically Scanned Antennas, IEE Colloquium on*, 21 Jan. 1988. (pp. 4/1 – 4/4)

[33] P. V. Brennan and A. W. Houghton," Phased array beam steering using phase-locked loops," *Electron. Lett.*, vol. 26, no. 3, pp. 165-166, 1st Feb. 1990.

[34] M. –Y. Li and K. Chang," New tunable phase shifters using perturbed dielectric image lines," *IEEE Trans. Microwave Theory and Tech.*, MTT-46, no. 10, pp. 1520-1523, Oct. 1998.

[35] P. M. Backhouse, N. Apsley, C. Rogers and S. Jones," Antenna-coupled microwave phase shifters using GaAs varactors," *Electron. Lett.*, vol. 27, no. 6, pp. 491-492, 14th Mar. 1991.

[36] J. R. James, G. D. Evans and A. Frag," Beam scanning microstrip arrays using diodes," *IEE Proceedings –H*, vol. 140, no. 1, pp. 43-51, Feb. 1993.

[37] G. D. Evans, J. R. James, A. Henderson and A. Frag," Prospects for varactor scanning microstrip arrays," *Flat Plate and Low Profile Mobile Antennas, IEE Colloquium on*, 1990. (pp. 10/1-10/3)

[38] R. E. Horn, H. Jacobs, E. Freibergs and K. L. Klohn," Electronic modulated beam-steerable silicon waveguide array antenna," *IEEE Trans. Microwave Theory and Tech.*, MTT-28, pp. 647-653, Jun. 1980.

[39] F. K. Schwering and S. –T. Peng," Design of dielectric grating antennas for millimeter-wave applications," *IEEE Trans. Microwave Theory and Tech.*, MTT-31, pp. 199-209, Feb. 1983.

[40] F. K. Schwering," Millimeter wave antennas," *IEEE Proceedings*, vol. 80, pp. 92-102, Jan. 1992.

[41] W. Menzel," A new travelling-wave antenna in microstrip," *Arch. Elek. Übertragung*, vol. 33, pp. 137-140, Apr. 1979.

[42] G. –J. Chou and C. –K. C. Tzuang," Oscillator-type active integrated antenna: the leaky-mode approach," *IEEE Trans. Microwave Theory and*

Tech., vol. 44, pp. 2265-2272, Dec. 1996.

[43] C. –K. C. Tzuang and C. C. Lin,” Millimeter wave micro-CPW integrated antenna,” *Proc. SPIE Conf. on*, Denver, Colorado, USA, Aug. 5-8, 1996, pp. 513-518.

[44] K. –F. Fuh and C. –K. C. Tzuang,” Magnetically scannable microstrip antenna employing a leaky gyromagnetic microstrip line,” *Electron. Lett.*, vol. 31, no. 16, pp. 1309-1310, 3rd Aug. 1995.

[45] Y. Qian and T. Itoh,” Progress in active integrated antennas and their applications,” *IEEE Trans. Microwave Theory and Tech.*, vol. 46, pp. 1891-1900, Nov. 1998.

[46] Y. –H. Chou and S. –J. Chung,” A new phase-shifterless scanning technique for a two-element active antenna array,” *IEEE Trans. Microwave Theory and Tech.*, vol. 47, pp. 243-246, Feb. 1999.

[47] M. –Y. Li and K. Chang,” Novel low-cost beam-steering techniques using microstrip patch antenna arrays fed by dielectric image lines,” *IEEE Trans. Microwave Theory and Tech.*, vol. 47, pp. 453-457, Mar. 1999.

[48] T. Tanaka, S. Egashira, A. Sakitani and M. Aikawa,” A novel design method of loaded beam tilting antenna – realizing desired beam tilting, high directive gain and low sidelobe level – ,” in *proc. Asia-Pacific Microwave Conference, 1998*, pp. 449-452.

[49] A. A. Oliner,” A new class of scannable millimeter wave antennas, “ in *Proc. 20th European Microwave Conf.*, Budapest, Hungary, Sept. 1990, pp. 95-104.

[50] C. C. Hu, C. F. Jou, J. J. Wu and S. T. Peng, ”Spatial power combining using linear leak-wave antenna array with two-dimensional beam-scanning capability,” in *Proc. Asia-Pacific Microwave Conf. 1998*, pp. 909-910.

[51] C.-C. Chen and C.-K. C. Tzuang, “Phase-shifterless beam-steering micro-slotline antenna,” *Electronics Letters*, 11th April 2002, vol. 38, no. 8, pp. 354-355.

[52] T. Itoh, “Generalized spectral domain method for multiconductor printed lines and its applications to tunable suspended microstrips,” *IEEE Trans. Microwave Theory and Tech.*, vol. MTT-26, pp. 983-987, Dec. 1978.

[53] H. Kamitsuna, “A very small, low-loss MMIC rat-race hybrid using elevated coplanar waveguides,” *IEEE Microwave Guided Wave Lett*., vol. 2, pp. 337–339, Aug. 1992.

[54] W. R. Eisenstadt and Y. Eo, “S-parameter-based IC interconnect transmission line characterization,” *IEEE Trans. Comp., Hybrids, Manufact. Technol.*, vol. 15, pp. 483-490, Aug. 1992.

[55] K. C. Gupta, R. Garg, I. Bahl, and P. Bhartia, *Microstrip Lines and Slotlines*. Norwood, MA: Artech House, 1996, pp. 189-194.

[56] C.–K. C. Tzuang, C.–C. Chen, and W.–Y. Chien, “LC-free CMOS oscillator employing two-dimensional transmission line,” *in Proc. IEEE Int. Frequency Control Symp. and PDA Exhibition/17th Euro. Frequency and Time Forum*, 2003, pp. 487-489.

[57] G. J. Chou, and C.–K. C. Tzuang, “An integrated quasi-planar leaky-wave antenna,” *IEEE Trans. Antennas Propagat.*, AP-44, pp. 1078-1085, Aug. 1996.

[58] G. J. Chou, and C.–K. C. Tzuang, “Oscillator-type active integrated antenna: the leaky-mode approach,” *IEEE Trans. Microwave Theory Tech.*, MTT-44, pp. 2265-2272, Dec. 1996.

[59] N. K. Das, “Spectral-domain analysis of complex characteristic impedance of a leaky conductor-backed slotline,” in *IEEE MTT-S Int. Microwave Symp. Dig.*, 1996, pp. 1791-1794.

[60] W. T. Lo, C.–K. C. Tzuang, S. T. Peng, and C. H. Lin, “Full-wave and experimental investigations of resonant and leaky phenomena of microstrip step discontinuity problems with and without top cover,” in *IEEE MTT-S Int. Microwave Symp. Dig.*, 1994, pp. 473-476.

[61] Guillermo Gonzales, *Microwave Transistor Amplifiers Analysis and Design*, Prentice-Hall Inc. Englewood Cliffs, chapter 2, 1997.

[62] K. Kurokawa, “Power waves and the scattering matrix,” *IEEE Trans. Microwave Theory Tech.*, vol. MTT-13, pp. 194-202, Mar. 1965.

[63] K. C. Gupta, R. Garg, and R. Chadha, *Computer-Aided Design of Microwave Circuits*, Artech House, c1981.

[64] Y. C. Shih and K. S. Kong, “ Accurate broadband characterization of transmission lines,” in *IEEE MTT-S Int. Microwave Symp. Dig., 1998*, pp. 933-936.

[65] R. A. Pucel, D. J. Masse, and C. P. Hartwig, “ Losses in microstrip,” *IEEE Trans. Microwave Theory Tech.*, MTT-16, pp. 342-350, Jun. 1968.

[66] M. E. Goldfarb, and A. Platzker,“ Losses in GaAs microstrip,” *IEEE Trans. Microwave Theory Tech.*, vol. 38, pp. 1957-1963, Dec. 1990.

[67] C. -K. C. Tzuang, C. –D. Chen, and S. –T. Peng, “ Full-wave analysis of lossy quasi-planar transmission line incorporating the metal modes,” *IEEE Trans. Microwave Theory Tech.*, vol. 38, pp. 1792-1799, Dec. 1990.

Appendix A: The extracting processes of the guiding properties, Z_c, loss, and SWF for a finite length TL

To obtain the complex propagation constant γ from the two-port scattering parameters of the through line, the complex characteristic impedance must be obtained beforehand in this dissertation. This can be achieved by respectively adding an open load and a short load at the output port of the microstrip [61]. The input impedance with open and short loads at the output port can be expressed as

$$Z_{in,open} = Z_c \cdot \coth \gamma \ell \tag{A-1}$$

$$Z_{in,short} = Z_c \cdot \tanh \gamma \ell \tag{A-2}$$

Z_c is the complex characteristic impedance of the transmission line with complex propagation constant γ and length ℓ.

Let Z_o be the reference impedance level, normally 50 Ω in a typical S-parameter measurement system, the two-port scattering matrix $\underline{\underline{S}}$ can be related to $Z_{in,open}$ and $Z_{in,short}$ by the following expressions[61],

$$Z_{in,open} = Z_o \cdot \frac{1 + S_{11}'(\infty)}{1 - S_{11}'(\infty)} \tag{A-3}$$

$$Z_{in,short} = Z_o \cdot \frac{1+S_{11}'(0)}{1-S_{11}'(0)} \tag{A-4}$$

where

$$S_{11}'(\infty) = S_{11} + \frac{S_{12}S_{21}}{1-S_{22}} \tag{A-5}$$

$$S_{11}'(0) = S_{11} - \frac{S_{12}S_{21}}{1+S_{22}} \tag{A-6}$$

S_{11}, S_{12}, S_{21} and S_{22} are the elements of the two-port $\underline{\underline{S}}$ - parameters referenced to Z_o. It should be noticed that $S_{11} = S_{22}$ and $S_{12} = S_{21}$ for symmetrical and passive circuits.

Substituting equations (A-3), (A-4), (A-5) and (A-6) into equations (A-1) and (A-2), the complex characteristic impedance Z_c can be solved as follows:

$$Z_c = Z_o \cdot \sqrt{\frac{1+S_{11}'(\infty)}{1-S_{11}'(\infty)} \cdot \frac{1+S_{11}'(0)}{1-S_{11}'(0)}} \tag{A-7}$$

For symmetrical and passive circuits, the $S_{11} = S_{22}$ and $S_{12} = S_{21}$ substitute into Eq. (A-5)-(A-7), then we can get the simplified formula of Z_c that shows as (3.6).

The scattering matrix $\underline{\underline{S}}$ is then re-normalized to Z_c^* and Z_c for the input port-1 and the output port-2, respectively [62], where the Z_c^* is the conjugate of

the Z_c, and the resultant scattering matrix $\underline{\underline{S_p}}$ $\left(\begin{bmatrix} S_{p11} & S_{p12} \\ S_{p21} & S_{p22} \end{bmatrix}\right)$ should have the following characteristics

$$S_{p11} = 0 \tag{A-8}$$

$$S_{p21} = e^{-\gamma \cdot \ell} \tag{A-9}$$

The detail derivation of Eq. (A-8) and Eq. (A-9) will be given in the ***Appendix B*** of this dissertation, assuming that the guiding transmission line under investigation supports only a bound mode with characteristic impedance Z_c and propagation constant γ. After invoking the complex impedance re-normalization process, the complex propagation constant γ ($\gamma = \alpha + j\beta$) becomes [8]

$$\alpha / k_o = \left(\frac{-\ln |S_{p21}|}{\ell} \right) / k_o \tag{A-10}$$

$$\beta / k_o = \sqrt{\varepsilon_{r,eff}} = \arg(S_{p21}) \cdot \frac{c}{2\pi f \cdot \ell} \tag{A-11}$$

Where α is the attenuation constant (unit = Np/m), k_o is the free-space wave number ($=\frac{2\pi}{\lambda_o}$ or $\frac{2\pi f}{c}$), $|S_{p21}|$ is the magnitude of S_{p21}, ℓ is the length of the equivalent transmission line (unit = m), β is the phase constant (unit = rad/m),

$\varepsilon_{r,eff}$ is the effective relative dielectric constant of the transmission line, arg(S_{p21}) is the total delay phase of S_{p21} (unit = rad), c is the speed of light ($\approx 3\times10^8$ m/sec) and f is the operating frequency(unit = Hz).

The guiding properties of a transmission line can be fully characterized by impedance characteristic ($Z_c(f)$) and dispersion characteristic ($\gamma(f)=\alpha(f)+j\beta(f)$). However, the relative parameters of loss per guided-wavelength (*Loss* (dB/λ_g)) and slow-wave factor (*SWF* = λ_0/λ_g = β/k_o) bear more meaning for slow-wave structures. The characteristic impedance, loss per guided-wavelength, and slow-wave factor can be obtained from Eqs. (A-7), (A-10) and (A-11). Moreover, *Loss*(dB/λ_g) and *SWF* can also be expressed as follows:

$$Loss(dB/\lambda_g) = 20\cdot\log_{10}(e^{-\alpha\cdot\lambda_g}) = 10^3\cdot Loss(dB/mm)\cdot\lambda_g \quad \text{(A-12)}$$

$$\text{SWF} = \frac{\lambda_0}{\lambda_g} = \frac{\beta}{k_0} = \sqrt{\varepsilon_{r,eff}} \quad \text{(A-13)}$$

where α is the attenuation constant (unit =$1/m$), λ_g is the guided-wavelength (unit = m), and $Loss(dB/mm) = 20\cdot\log_{10}(e^{-0.001\cdot\alpha})$.

The guiding properties (Z_c, SWF, and loss) are extracted directing from the S-parameter of the simulated or measured DUT transmission line (MS, CCS,...). The extracting processes can be summarized as follows:

Step1: properly choose the length ℓ of transmission line, that $\ell < 0.25\lambda_g$ is suggested, else the extracting parameters will be caused by large disturbance near those frequencies where the line length $\ell = \frac{n}{2} \cdot \lambda_g$, n = 1, 2, 3, etc., and λ_g is the guided-wavelength of transmission line. The spurious resonance and numerical error are severely and obviously as the line length ℓ near to a multiple of half-guided-wavelength. The numerical method to reduce the error will be listed in Appendix C.

Step2: to get its two-port scattering parameters [S] reference to $Z_{o,}$ normally 50-Ω, by simulation or measurement,

Step3: at first, to decide the characteristic impedance of the transmission line, Z_c, that is derived from the input impedance with open and short loads at the output port, the final expression is

$$Z_c = \sqrt{Z_{in,open} \cdot Z_{in,short}} = Z_o \cdot \sqrt{\frac{1+S_{11}'(\infty)}{1-S_{11}'(\infty)} \cdot \frac{1+S_{11}'(0)}{1-S_{11}'(0)}}$$

Where $S_{11}'(\infty) = S_{11} + \frac{S_{12}S_{21}}{1-S_{22}}$ and $S_{11}'(0) = S_{11} - \frac{S_{12}S_{21}}{1+S_{22}}$,

the $S_{11} = S_{22}$ and $S_{12} = S_{21}$ for symmetrical and passive circuits,

Step4: to perform the re-normalized process, to the scattering matrix [S], that is

re-normalized to Z_c^* and Z_c for the port-1 and port-2, respectively.

The resultant scattering matrix S_p $\left(\begin{bmatrix} S_{p11} & S_{p12} \\ S_{p21} & S_{p22} \end{bmatrix}\right)$

where $S_{p11} = 0$, $S_{p21} = e^{-\gamma\ell}$ and $\gamma = \alpha + j\beta$, γ: propagation constant, α: attenuation constant, β: phase constant,

Step5: to extract the normalized propagation constant γ/k_o (α/k_o, β/k_o) from the S_{p21},

$$\alpha / k_o = \left(\frac{-\ln |S_{p21}|}{\ell} \right) / k_o$$

$$\beta / k_o = \sqrt{\varepsilon_{r,eff}} = \arg(S_{p21}) \cdot \frac{c}{2\pi f \cdot \ell}$$

where $|\boldsymbol{S_{p21}}|$ is the insertion loss and $\arg(\boldsymbol{S_{p21}})$ is the delay-phase of transmission line, at the condition, $Z_s = Z_c^*$ for the input port-1 and $Z_L = Z_c$ for the output port-2.

Step6: to extract the ***Loss (dB/λ_g)*** and ***SWF*** from the α, $\boldsymbol{\lambda_g}$**, and** β/k_o**,**

$$Loss(dB/\lambda_g) = 20 \cdot \log_{10}(e^{-\alpha \cdot \lambda_g}) = 10^3 \cdot Loss(dB/mm) \cdot \lambda_g$$

$$\text{SWF} = \frac{\lambda_0}{\lambda_g} = \frac{\beta}{k_0} = \sqrt{\varepsilon_{r,eff}}$$

Appendix B: The derivation of the power-wave scattering parameter matrix, $\underline{\underline{S_p}}$, for a finite length TL with complex reference impedances Z_1 and Z_2

The propagation characteristics of the finite length transmission line can be characterized by Z_c (complex characteristic impedance), γ (= α +j β, complex propagation constant, where α is the attenuation constant and β is the phase constant), and ℓ (length of the transmission line) using two-port transmission line circuit model, $\begin{bmatrix} A & B \\ C & D \end{bmatrix}$ matrix.

The equivalent circuit of this model is shown as follows,

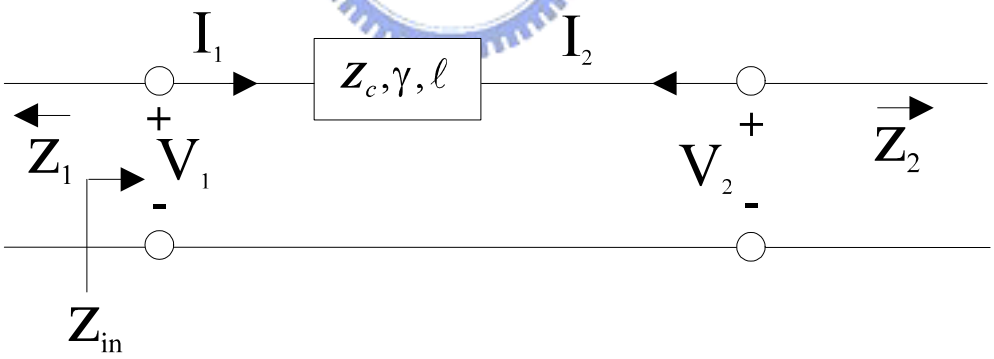

Fig. B-1. The equivalent circuit model of the two-port TL.

Where I_1, V_1 and I_2, V_2 are expressed as terminated current and voltage at port-1 and port-2, respectively.

Equation (B-1) formulizes the relation between these 2 ports [61], [63],

$$\begin{bmatrix} V_1 \\ I_1 \end{bmatrix} = \begin{bmatrix} A & B \\ C & D \end{bmatrix} \cdot \begin{bmatrix} V_2 \\ -I_2 \end{bmatrix} \tag{B-1}$$

Where $\begin{bmatrix} A & B \\ C & D \end{bmatrix}$ is equal $\begin{bmatrix} \cosh \gamma \ell & Z_c \cdot \sinh \gamma \ell \\ \frac{1}{Z_c} \cdot \sinh \gamma \ell & \cosh \gamma \ell \end{bmatrix}$.

The input impedance Z_{in}(=V_1/I_1) can be derived from Eq. (B-1) as follows,

$$Z_{in} = Z_c \cdot \frac{Z_2 \cdot \cosh \gamma \ell + Z_c \cdot \sinh \gamma \ell}{Z_c \cdot \cosh \gamma \ell + Z_2 \cdot \sinh \gamma} \tag{B-2}$$

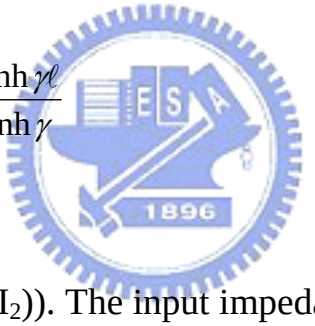

Where Z_2 is equal to ($V_2/(-I_2)$). The input impedance Z_{in} (=V_1/I_1) is equal to Z_c as Z_2 (=$V_2/(-I_2)$) is equal to Z_c.

From Eq. (B-1) and Fig. (B-1) we have,

$$V_1 = AV_2 - BI_2 \tag{B-3}$$

$$I_1 = CV_2 - DI_2 \tag{B-4}$$

$$V_1 = -I_1 Z_1 \tag{B-5}$$

$$V_2 = -I_2 Z_2 \tag{B-6}$$

On the other hand, the definition of the incident and reflected power waves a_i and b_i, i =1, 2 for port-1, port-2, indicates that [62]

$$a_i = \frac{V_i + Z_i \cdot I_i}{2 \cdot \sqrt{|\mathrm{Re}(Z_i)|}} \equiv \frac{V_i + Z_i \cdot I_i}{2 \cdot \hat{Z}_i} \tag{B-7}$$

$$b_i = \frac{V_i - Z_i^* \cdot I_i}{2 \cdot \sqrt{|\mathrm{Re}(Z_i)|}} \equiv \frac{V_i - Z_i^* \cdot I_i}{2 \cdot \hat{Z}_i} \tag{B-8}$$

Where $|\mathrm{Re}(Z_i)|$ is the magnitude of the real part of Z_i, $\hat{Z}_i$ is defined as the square root of $|\mathrm{Re}(Z_i)|$, and Z_i^* is the conjugate of Z_i.

From Eq. (B-7) and Eq. (B-8), we can solve V_1 and I_1 in terms of a_1 and b_1 for port-1 by the following formula,

$$V_1 = \frac{(Z_1^* \cdot a_1 + Z_1 \cdot b_1) \cdot \hat{Z}_1}{\mathrm{Re}(Z_1)} \tag{B-9}$$

$$I_1 = \frac{(a_1 - b_1) \cdot \hat{Z}_1}{\mathrm{Re}(Z_1)} \tag{B-10}$$

Similarly we can solve V_2 and $(-I_2)$ in terms of a_2 and b_2 for port-2 by the

following formula,

$$V_2 = \frac{(Z_2^{*} \cdot a_2 + Z_2 \cdot b_2) \cdot \hat{Z}_2}{\mathrm{Re}(Z_2)} \tag{B-11}$$

$$-I_2 = \frac{-(a_2 - b_2) \cdot \hat{Z}_2}{\mathrm{Re}(Z_2)} \tag{B-12}$$

Equation (B-9) to (B-12) can be rearranged in matrix form as follows,

$$\begin{bmatrix} V_1 \\ I_1 \end{bmatrix} = \begin{bmatrix} \frac{Z_1^{*} \cdot \hat{Z}_1}{\mathrm{Re}(Z_1)} & \frac{Z_1 \cdot \hat{Z}_1}{\mathrm{Re}(Z_1)} \\ \frac{\hat{Z}_1}{\mathrm{Re}(Z_1)} & \frac{-\hat{Z}_1}{\mathrm{Re}(Z_1)} \end{bmatrix} \cdot \begin{bmatrix} a_1 \\ b_1 \end{bmatrix} \equiv \underline{\underline{U}}_1 \cdot \begin{bmatrix} a_1 \\ b_1 \end{bmatrix} \tag{B-13}$$

$$\begin{bmatrix} V_2 \\ -I_2 \end{bmatrix} = \begin{bmatrix} \frac{Z_2^{*} \cdot \hat{Z}_2}{\mathrm{Re}(Z_2)} & \frac{Z_2 \cdot \hat{Z}_2}{\mathrm{Re}(Z_2)} \\ \frac{-\hat{Z}_2}{\mathrm{Re}(Z_2)} & \frac{\hat{Z}_2}{\mathrm{Re}(Z_2)} \end{bmatrix} \cdot \begin{bmatrix} a_2 \\ b_2 \end{bmatrix} \equiv \underline{\underline{U}}_2 \cdot \begin{bmatrix} a_2 \\ b_2 \end{bmatrix} \tag{B-14}$$

Substituting Eq. (B-13) and (B-14) into Eq. (B-1), we have

$$\underline{\underline{U}}_1 \cdot \begin{bmatrix} a_1 \\ b_1 \end{bmatrix} = \begin{bmatrix} A & B \\ C & D \end{bmatrix} \cdot \underline{\underline{U}}_2 \cdot \begin{bmatrix} a_2 \\ b_2 \end{bmatrix} \tag{B-15}$$

$$\Rightarrow \begin{bmatrix} a_1 \\ b_1 \end{bmatrix} = \underline{\underline{U}}_1^{-1} \cdot \begin{bmatrix} A & B \\ C & D \end{bmatrix} \cdot \underline{\underline{U}}_2 \cdot \begin{bmatrix} a_2 \\ b_2 \end{bmatrix} \equiv \begin{bmatrix} V_{11} & V_{12} \\ V_{21} & V_{22} \end{bmatrix} \cdot \begin{bmatrix} a_2 \\ b_2 \end{bmatrix} \equiv \underline{\underline{V}} \cdot \begin{bmatrix} a_2 \\ b_2 \end{bmatrix} \tag{B-16}$$

$$\Rightarrow \begin{bmatrix} b_1 \\ b_2 \end{bmatrix} = \begin{bmatrix} \frac{V_{22}}{V_{12}} & \frac{-\det(\underline{\underline{V}})}{V_{12}} \\ \frac{1}{V_{12}} & \frac{-V_{11}}{V_{12}} \end{bmatrix} \cdot \begin{bmatrix} a_1 \\ a_2 \end{bmatrix} \equiv \begin{bmatrix} S_{p11} & S_{p12} \\ S_{p21} & S_{p22} \end{bmatrix} \cdot \begin{bmatrix} a_1 \\ a_2 \end{bmatrix} \equiv \underline{\underline{S_p}} \cdot \begin{bmatrix} a_1 \\ a_2 \end{bmatrix} \quad \text{(B-17)}$$

Where $\underline{\underline{S_p}}$ is the power-wave scattering parameter matrix that is referred to the reference impedance Z_1 and Z_2 at port-1 and port-2, respectively, $\det(\underline{\underline{V}}) = (V_{11} \cdot V_{22} - V_{12} \cdot V_{21})$.

Assume the system under consideration is reciprocal and passive, where $\mathrm{Re}(Z_1)$, $\mathrm{Re}(Z_2)$ are positive and Z_1, Z_2 are complex, the scattering parameters of the matrix $\underline{\underline{S_p}}$ can be found by the following equations,

$$S_{p11} = \left(\frac{Z_2 \cdot \cosh\gamma\ell - \frac{Z_1^{\,*} \cdot Z_2}{Z_c} \cdot \sinh\gamma\ell + Z_c \cdot \sinh\gamma\ell - Z_1^{\,*} \cdot \cosh\gamma\ell}{Z_2 \cdot \cosh\gamma\ell + \frac{Z_1 \cdot Z_2}{Z_c} \cdot \sinh\gamma\ell + Z_c \cdot \sinh\gamma\ell + Z_1 \cdot \cosh\gamma\ell} \right) \quad \text{(B-18)}$$

$$S_{p21} = \left(\frac{2 \cdot \hat{Z}_1 \cdot \hat{Z}_2}{Z_2 \cdot \cosh\gamma\ell + \frac{Z_1 \cdot Z_2}{Z_c} \cdot \sinh\gamma\ell + Z_c \cdot \sinh\gamma\ell + Z_1 \cdot \cosh\gamma\ell} \right) = S_{p12} \quad \text{(B-19)}$$

where $-\det(\underline{\underline{V}}) = 1$,

$$S_{p22}=\left(\frac{-Z_2^{*}\cdot\cosh\gamma\ell-\frac{Z_1\cdot Z_2^{*}}{Z_c}\cdot\sinh\gamma\ell+Z_c\cdot\sinh\gamma\ell+Z_1\cdot\cosh\gamma\ell}{Z_2\cdot\cosh\gamma\ell+\frac{Z_1\cdot Z_2}{Z_c}\cdot\sinh\gamma\ell+Z_c\cdot\sinh\gamma\ell+Z_1\cdot\cosh\gamma\ell}\right) \quad \text{(B-20)}$$

The above scattering parameters can be further simplified for the following two cases:

Case1: $Z_1 = Z_2 = Z_c \equiv R_c + jX_c$

$$S_{p11}=\frac{jX_c}{R_c+jX_C}=S_{p22}\ ,\quad S_{p21}=\left(\frac{R_c}{R_c+jX_c}\right)\cdot e^{-\gamma\ell}=S_{p12} \quad \text{(B-21)}$$

For its special case of positive and real characteristic impedance, $Z_c = R_c$ and $X_c = 0$,

$$S_{p11}=S_{p22}=0\,,\quad S_{p21}=S_{p12}=e^{-\gamma\ell} \quad \text{(B-22)}$$

Case2: $Z_2 = Z_c$ and $Z_1 = Z_c^{*}$

$$S_{p11}=0\,,\ S_{p21}=S_{p12}=e^{-\gamma\ell}\ ,\quad S_{p22}=\left(\frac{jX_c}{R_c+jX_c}\right)\cdot\left(1-e^{-2\gamma\ell}\right) \quad \text{(B-23)}$$

After the characteristic impedance Z_c of the transmission line is found, the new parameters S_p can be obtained by changing the original 50-ohm ($Z_1 = Z_2 = 50\ ohm$) system to the new complex impedance ($Z_1^* = Z_2 = Z_c$) system. Secondly, we can directly extract the loss and slow-wave factor (SWF) parameters from the magnitude and phase of S_{p21} as Eq. (A-10) to Eq. (A-13).

Appendix C: Using numerical technique to obtain accurate broadband characterization of TL

The results of the guided properties from S-parameter 3D Full-Wave analyses and measurement may exist larger error as the length ℓ of the Device-Under-Testing (DUT) transmission line equals to the multiple of half-wave-length. The relatively large error in the characteristic impedance values, except that due to the junction structural and/or electrical discontinuities, spurious resonance influence, and measurement uncertainties [64], [65], is mainly caused by numerical error. For example, the characteristic impedance Z_c can be found symbolically from Eq. (A-7), the expression $\left(\frac{1+S'_{11\_\inf}}{1-S'_{11\_zero}}\right)$ is numerically closely to $\left(\frac{2}{2}\right)=1$, and the expression $\left(\frac{1+S'_{11\_zero}}{1-S'_{11\_\inf}}\right)$ is numerically closely to $\left(\frac{0}{0}\right)$ at frequencies where the line length $\ell \sim \frac{n}{2}\lambda_g$, n = 1, 2, 3, … and so on, λ_g is guided wavelength. Therefore a small variation in the denominator and/or numerator, such as $\pm 1\%$ error in the S'_{11_zero} (ex. -0.98 to -0.99) and $S'_{11\_\inf}$ (ex. 0.99 to 0.98), will cause about $\pm 35\%$ relatively large variation in Z_c (ex. $1.414 \cdot Z_o$ to $0.707 \cdot Z_o$) in numerical simulations. The extraction of the guided properties, *SWF* $(=\beta/k_o)$ and *Loss* (dB/λ_g), will also cause some degree error at frequencies where the line length ℓ is near a multiple of

half-wave-length.

For the special accuracy problem encounters with Z_c, *SWF* and *Loss* (dB/λ_g), we present here a numerical method to reduce the error. The procedures are described as follows:

Using well-known numerical curve fitting and interpolation technique, such as cubic-spline interpolation, we inserted as many data (2-port S-parameter) as possible in the variation frequency band, where the line length ℓ is near a multiple of half-wave-length.

We find out the error dominating frequencies where the line length $\ell = \frac{n}{2}\lambda_g$, n = 1, 2, 3, …and so on. From these data where the phase delay get from the parameter $\angle S_{p21}$ (or $\angle S_{21}$) are equal or most near to a multiple of 180° and the values of relative expression $(1+S'_{11\_zero})$, $(1-S'_{11\_\inf})$ are equal or most near to zero.

We delete all interpolated data except those in the error dominating frequencies. Let x_{on}, n = 1, 2, 3, …etc., be those data with respect to the frequency condition of the line length $\ell = \frac{n}{2}\lambda_g$, n = 1, 2, 3, …and so on.

The waiting processed data curves, the values of the real parts and the imaginary parts of the $(1+S'_{11\_zero})$, $(1-S'_{11\_inf})$ near at x_{o1}, x_{o2}, x_{o3}, etc., can be replaced approximately using n_i –order power series polynomial, respectively. Where the n_i –order is decided from the variation range of the guided properties (Z_c, *SWF* and *Loss* (dB/λ_g)), and the power series polynomial form is similar with Taylor series expansion to $x_{on,}$ which shows as following general expression,

$$f(x) = f(x_{on}) + a_{f1}\cdot(x-x_{on}) + a_{f2}\cdot(x-x_{on})^2 + ... + a_{fn_i}\cdot(x-x_{on})^{n_i} \qquad \text{(C-1)}$$

Where the symbol x represent frequency variable of variation range near x_{on}; $f(x_j)$ is the response value of $f(x)$ at $x = x_j$ for j = 1, 2, 3, … n_i and $x_1 < x_2 < x_3 \ldots < x_{n_i}$; the a_{f1}, a_{f2}, a_{f3}, … and a_{fn_i} are the constant coefficient of the first-order, the second-order, the third-order, …, and the n_i –order item, respectively. The constant coefficient a_{fj} can be solved from n_i simultaneous equations as follows:

$$[D] \equiv \begin{bmatrix} f(x_1)-f(x_{on}) \\ f(x_2)-f(x_{on}) \\ \vdots \\ f(x_{n_i})-f(x_{on}) \end{bmatrix} = \begin{bmatrix} (x_1-x_{on}) & (x_1-x_{on})^2 & \cdots & (x_1-x_{on})^{n_i} \\ (x_2-x_{on}) & (x_2-x_{on})^2 & \cdots & (x_2-x_{on})^{n_i} \\ \vdots & \vdots & \vdots & \vdots \\ (x_{n_i}-x_{on}) & (x_{n_i}-x_{on})^2 & \cdots & (x_{n_i}-x_{on})^{n_i} \end{bmatrix} \begin{bmatrix} a_{f1} \\ a_{f2} \\ \vdots \\ a_{fn_i} \end{bmatrix} \equiv [C]\cdot[A]$$

So,

$$[A] = [C]^{-1} \cdot [D] \tag{C-2}$$

Where the matrix [*A*] is the constant coefficient matrix.

Theoretically, when *x* is equal to x_{on}, $f(x) = f(x_{on})$ is equal to zero for n=1, 2, 3, and so on. In physically, the numerical-error results display that only close to zero in some degree. Assuming that

$$V(x) \equiv \left(\frac{1 + S'_{11\_\inf}(x)}{1 - S'_{11\_zero}(x)} \right) \tag{C-3}$$

and

$$U(x) \equiv \left(\frac{1 + S'_{11\_zero}(x)}{1 - S'_{11\_\inf}(x)} \right) \equiv \left(\frac{F_r(x) + j \cdot F_i(x)}{G_r(x) + j \cdot G_i(x)} \right) \tag{C-4}$$

Where the $F_r(x)$, $F_i(x)$, $G_r(x)$, and $G_i(x)$ all can be represented by Eq. (C-1), the relative coefficients can also be solved in according with the procedures of Eq. (C-2).

When the a_{f1}, a_{f2}, a_{f3}, ……., and a_{fn_i} have been resolved in Eq. (C-1), the mainly processed procedures display as follows:

The first, to process the characterization variation frequency points except for at $x = x_{o1}, x_{o2}, x_{o3}, \ldots$etc. Setting the numerical error $f(x_{on})$ to zero in Eq. (C-1), to get the modified new values of $f(x)$, applying to the $F_r(x)$, $F_i(x)$, $G_r(x)$, $G_i(x)$ near at $x_{o1}, x_{o2}, x_{o3}, \ldots$ etc., respectively, to get the modified new values of $U(x)$ and the relative values of $V(x)$, to solve the modified new characteristic impedance $Z_c(x)$.

The second, to process the error dominating frequency points at $x = x_{o1}, x_{o2}, x_{o3}, \ldots$etc. Here, $U(x)$ occur $\left(\frac{0}{0}\right)$ at $x = x_{o1}, x_{o2}, x_{o3}, \ldots$etc., to solve the limitation values of $U(x)$ as x approach to the $x_{o1}, x_{o2}, x_{o3}, \ldots$etc., respectively, in according with L'Hopital's rule, to get the modified new values of $U(x)$ and the relative values of $V(x)$, to solve the modified new $Z_c(x)$ at $x = x_{o1}, x_{o2}, x_{o3}...$, respectively.

Finally, using the modified new Z_c to get the other guiding properties (*SWF* and *Loss* (dB/λ_g)) of transmission line in according with the γ - extracting procedures from Eqs. (A-8) - (A-13) in Appendix A.

For verified purpose, we have used above numerical method and extracting procedures, to process simulated and/or measured S-parameter of a finite length

traditional MS line, to solve its characterization ($Z_{c,}$ β/k_{o0} = *SWF,* α/k_o, *Loss (dB/mm), and Loss (dB/*λ_g*)… etc.*). We have also applied the presented numerical method to process the original values of characteristic impedance Z_c, to reduce the influence of numerical error near at frequencies where the line length $\ell = \frac{n}{2}\lambda_g$, n = 1, 2, 3, …etc., to get the accurate broadband characterization of transmission line ($Z_{c,}$ *SWF, and Loss(dB/*λ_g*)*). These examples will be presented and discussed as Appendix D.

Appendix D. Verified Examples of the γ - Z_c Extracting Procedure and Numerical Technique for the finite-length TL

Case 1:

The measured results across the 5 GHz to 40 GHz band reported by Goldfard and Platzker [66, Fig. 8] are applied to validate the above-mentioned theoretical extracting procedure for obtaining Z_c and γ.

First, the measured data by Goldfard and Platzker are validated by the mode-matching method (MMM) incorporating the metal mode [67] as shown Fig. D-1(a). Then the full-wave method-of-moment (MOM) results are compared to the MMM data in Fig. D-1(b). Figure D-1(a) shows that the attenuation constants (in dB/mm) obtained by the MMM are in the middle of error bound when operating frequency is below 10 GHz. By contrast the attenuation constants approach the lower limit of the error bound between 10 GHz and 35 GHz. The attenuation constants obtained by the full-wave MOM are slightly below the measurement limits of error below 25 GHz and approach upper limit near 35 GHz. Since the MMM data agree very well with the measurement across the band, they are used as a reference to access the accuracy of the full-wave MOM extracting procedure. Figure D-1(b) indicates that the normalized attenuation constant (α/k_o) obtained by the full-wave MOM is

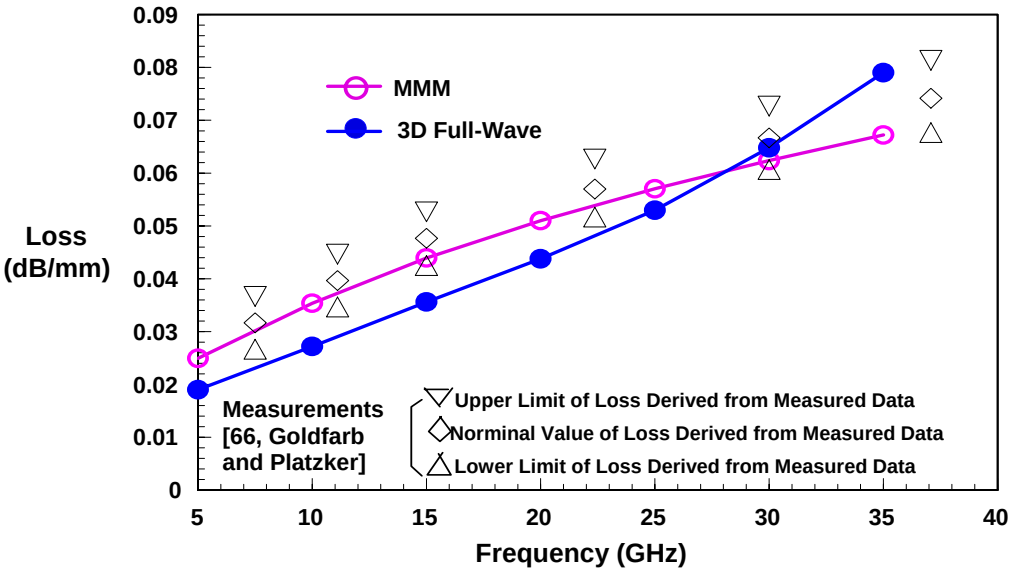

approximately –23.77 % at 5

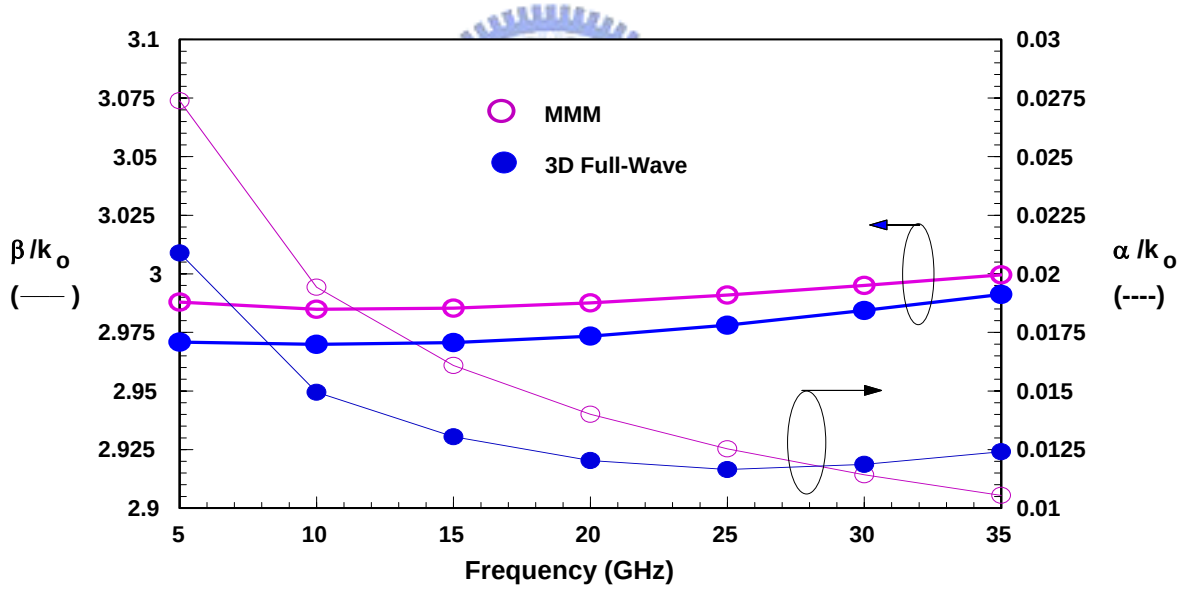

(a) *Loss (dB/mm)* vs. *f*

(b) Dispersion characteristics: (β/k) ,(α/k_o) vs. *f*

Fig. D-1. The comparison of losses in GaAs MS for 70-μm width on 100-μm GaAs, using the MMM and 3D Full-Wave MOM Integral Equations. (a) *The*

losses, using MMM and *3D* Full-Wave simulations, compare to previous work [66], (b) The dispersion characteristics β / k (solid lines) and α / k_o (dash lines) versus *frequency*.

GHz and 17.54 % at 35 GHz less than those obtained by the MMM. On the other hand, the maximum deviation of the normalized phase constant (β/k_o) between two method occurs at the lowest frequency end at 5GHz, where only –0.57 % deviation from the MMM data is observed. Therefore the validity of the full-wave MOM parameters extracting procedure is validated, provided approximately ± 20 % error bound is acceptable for the normalized attenuation constant across the band.

Case 2:

Here, we present an example of a traditional MS line structure that Roger RO4003 substrate of thickness of 0.508 mm, relative dielectric constant ε_r of 3.38, tan-loss $tan\delta$ of 0.0022, and cladding conductor thickness of 17.5 μm is employed for the 110-Ω MS line design. The MS line structural parameters are linewidth W of 0.278 mm, ground-plane width of 1.524 mm, and line length *L* of 48.379 mm.

The comparing guiding property parameters: characteristic impedance (Z_{co} and Z_c), slow-wave factor (*SWF*) and loss per guided wavelength (*Loss (dB/*λ_g*)*) versus frequency that got from the original data characteristic impedance Z_{co} and the numerical method processed characteristic impedance Z_c for the conventional MS line, show as Fig. D-2(a)-(b).

We find out the original data Z_{co} have larger variation near about at 7.8 GHz (L ~ 0.5 λ_g), which the curve of the real parts Re(Z_{co}) has a tip (~ 131 Ω) about at 7.7 GHz and a dip (~ 82 Ω) about at 7.8 GHz, simultaneously, the curve of the imaginary parts Im(Z_{co}) has a dip (~ -17.5 Ω) about at 7.8 GHz, and the derived *SWF* and *Loss (dB/*λ_g*)* have a little variation about at 7.8 GHz that got from the Z_{co}. But the other hand, the processed characteristic impedance Z_c by numerical

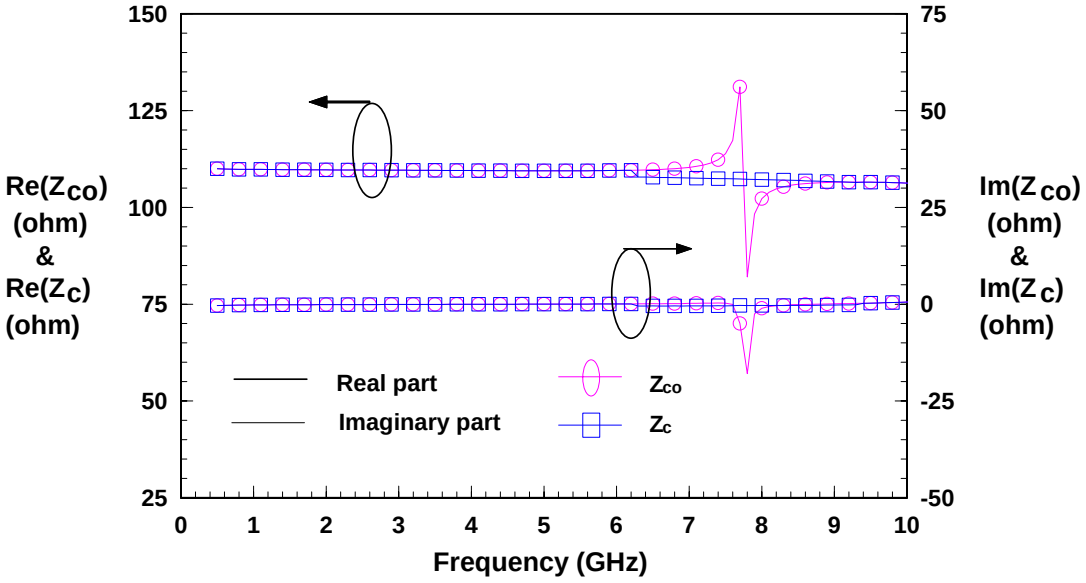

(a) Z_{co} and Z_c vs. f

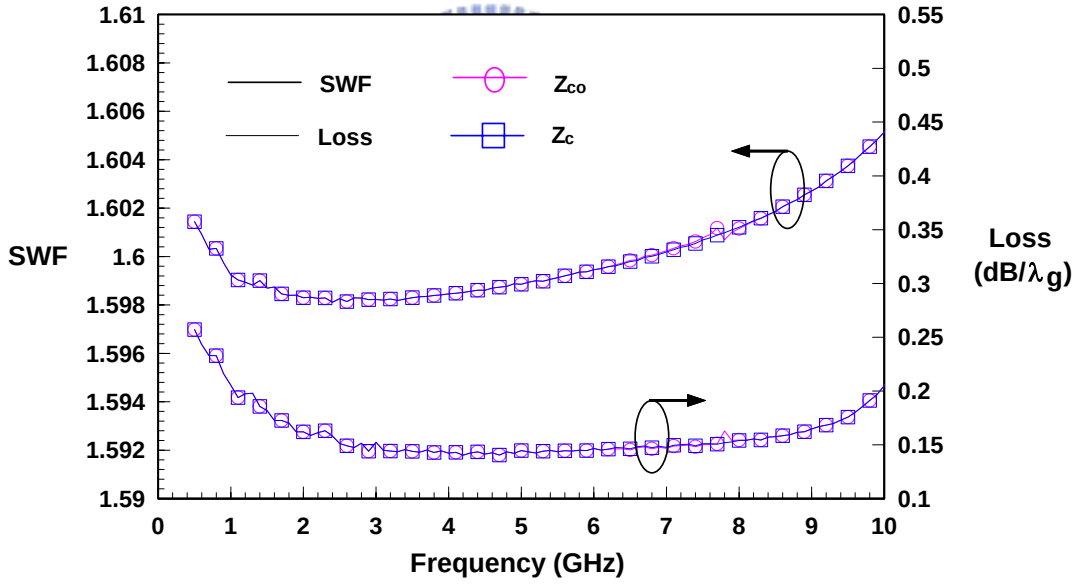

(b) *SWF* and *Loss(dB/* λ_g*)* vs. f

Fig. D-2. The Compare of guiding property parameters: (a) Z_{co} and Z_c versus *frequency*, (b) *SWF* and *Loss(dB/* λ_g*)* versus *frequency*, that got from the original data - characteristic impedance Z_{co} and the processed characteristic impedance Z_c by numerical technique, for conventional MS line.

technique are smoothly for real part and imaginary part and the derived *SWF* and *Loss (dB/λ_g)* are more smooth that got from the Z_c.

Beside, we derived the characteristic impedance (Z_c) that got from the input (or output) voltage standing-wave-ratio (VSWR) at the interested frequencies ($L = \frac{n}{4} \cdot \lambda_g$, n = 1, 2, 3…) [8] as following expression

$$Z_c = Z_o \cdot \sqrt{VSWR_{\max} \cdot VSWR_{\min}} \qquad \text{(D-1)}$$

Where the Z_o is equal to 50 Ω; the maximum VSWR, $VSWR_{max}$, is equal to 4.764 occur at 3.9 GHz (~ 0.25 λ_g) and the minimum VSWR, $VSWR_{min}$, is equal to 1.019 occur at 7.8 GHz (~ 0.5 λ_g), the characteristic impedance Z_c is approximately equal to 110.165 Ω for the case.

The error-percentage of the characteristic impedance Z_c that got from Eq. (D-1) comparing to our numerical method is smaller than 3.64 %. So, the validity of the presented numerical method for Z_c-parameter extraction is verified again.

Summary:

By comparing to the data that get from Mode-Match method (MMM) and HP ADS Line-CAL software analyses, the results are identically well and satisfied to our demand. So, the validity of presented numerical method and extraction procedures are verified.

In the following, we will apply the presented numerical method to process the original characteristic impedance Z_{co}, to reduce the serious influence of the numerical error near at $l = \frac{n}{2} \cdot \lambda_g$ and n = 1, 2, 3 etc., to get the broadband guided properties (Z_c, *SWF* and *Loss (dB/*λ_g*)*) of the TLs in this dissertation.